Available online at www.sciencedirect.com
SCIENCE DIRECT®
Catalysis Today 105 (2005) 551–559
CATALYSIS TODAY
www.elsevier.com/locate/cattod

The effect of support morphology on the reaction of oxidative dehydrogenation of ethane to ethylene at short contact times

Francesco Donsì [a,*], Stefano Cimino [b], Almerinda Di Benedetto [b], Raffaele Pirone [b], Gennaro Russo [a]

[a] *Department of Chemical Engineering, Università degli Studi di Napoli Federico II – P.le Tecchio 80, 80125 Napoli, Italy*
[b] *Istituto di Ricerche sulla Combustione, CNR, Italy*

Available online 11 July 2005

Abstract

The oxidative dehydrogenation of ethane is carried out in short contact time reactors over Pt and $LaMnO_3$ based catalysts supported on a large number of different ceramic substrates (45, 60 and 80 ppi foam monoliths and 200, 400, 600, 900 and 1200 cpsi honeycomb monoliths). Experimental results, obtained under the same conditions at varying the C_2H_6/O_2 ratio, showed that the highest performance in terms of ethylene selectivity and yield is always attained on $LaMnO_3$ catalysts. Furthermore, the results are significantly influenced by the morphology and cell density of the support, with 45 and 60 ppi foams and 400 and 600 cpsi honeycombs giving the best performance. The experimental results are explained by means of geometrical and fluid dynamic considerations on the support, and by means of a 2D mathematical model, which clearly indicates an optimal intermediate cell density for maximising ethylene selectivity and yield.

Keywords: Structured catalysts; Oxidative dehydrogenation; Pt; Perovskite; Support morphology; Ethylene

1. Introduction

The oxidative dehydrogenation (ODH) of ethane in short contact time reactors resulted a viable option for ethylene production with high yields [1]. The intrinsic nature of the process, characterized by the strict coupling between homogeneous and heterogeneous reactions, preferably requires structured reactors. For historical reasons, since it was first proposed in 1993, it was carried out mainly on foam monoliths [1]. Bodke et al. reported that support geometry might considerably affect the performance in the partial oxidation of light hydrocarbons for synthesis gas or olefins production with short contact time foam reactors. In order to maximise yields the authors recommended in either case the smallest possible pore size (80 ppi, among tested supports), as long as pressure drops are acceptable [2].

Honeycomb monoliths were employed by Sadykov et al. and Lødeng et al. under the mild conditions of propane ODH, with the motivation that the use of micro-monoliths with straight channels could reduce the extent of homogeneous reactions consuming propylene [3,4]. Recently we showed that the ODH of ethane can be carried out on $LaMnO_3$-based catalyst deposited on 400 cpsi honeycomb monoliths with very high ethylene yields [5,6], competitive with the industrial process of ethane steam cracking upon fuel addition (H_2 and CO) [7].

In this work, we extend the study of ethane ODH reaction on both $LaMnO_3$- and Pt-based catalysts by comparing the performance of the previously tested 400 cpsi monoliths with a large number of ceramic substrates (45, 60 and 80 ppi foam monoliths and 200, 600, 900 and 1200 cpsi honeycomb monoliths), with the aim of addressing a detailed comparison between two different monolith morphologies (foams and honeycombs), at varying the cell density.

2. Experimental

Incipient-wetness impregnation was used to deposit Pt directly onto bare macroporous ceramic monoliths (foams

* Corresponding author. Tel.: +39 081 7682947; fax: +39 081 5936936.
E-mail address: fradonsi@unina.it (F. Donsì).

0920-5861/$ – see front matter © 2005 Elsevier B.V. All rights reserved.
doi:10.1016/j.cattod.2005.06.016

45, 60 and 80 ppi; honeycombs 200, 400, 600, 900 and 1200 cpsi). The total loading of noble metal was increased proportionally to the increasing geometrical surface area of the substrate in order to keep a constant superficial density of active sites. $LaMnO_3$ perovskite was deposited by wet-impregnation onto an intermediate La_2O_3-stabilized γ-Al_2O_3 washcoat layer of constant average thickness (20 μm), which was anchored on selected monolithic substrates as previously described [7]. All the catalysts were calcined in air at 1000 °C for 3 h before testing. The catalytic monoliths, in the shape of disks of 17 mm diameter and 10 mm long, were stacked between two inert monoliths as radiation shields and placed in a quartz tube inserted in an electric furnace that was used only for igniting the reacting mixture. Further details on the experimental set up have been already reported elsewhere [6,7]. The comparison between Pt and $LaMnO_3$ was undertaken at varying C_2H_6/O_2 ratio between 1.5 and 2.5, maintaining constant N_2 dilution (30 vol.%) and the total flow rate at 50 slph (standard liters per hour), corresponding to a gas hourly space velocity (GHSV) of $2.4 \times 10^4\ h^{-1}$ and to a residence time of about 50 ms at an average reactor temperature of 900 °C. All results were checked twice for repeatability and carbon balance was always closed within 3%; the accuracy for ethylene measurement was estimated in ±0.5%.

2.1. Morphological and fluid dynamic considerations

Table 1 reports the geometrical characteristics and the corresponding axial and radial Peclet numbers and hydrodynamic length of the different supports tested.

The honeycomb ceramic monoliths reported in Table 1 are formed by bundles of straight and parallel channels, of square section in the case herein investigated, made by extrusion of cordierite ($2MgO{\cdot}2Al_2O_3{\cdot}5SiO_2$), provided by Saint-Gobain Ceramics (200 cpsi), Corning (400 cpsi) and NGK (600, 900 and 1200 cpsi).

Foam monoliths instead consist of a solid phase made of a network of interconnected struts and of a continuous void phase constituted by spherical-like cells connected through windows [8,9], made of mullite ($3Al_2O_3{\cdot}SiO_2$) provided by EcoCeramics (45 and 60 ppi) or α-Al_2O_3, provided by Vesuvius Hi-Tech (80 ppi).

Due to the different manufacture, foam monoliths can attain higher cell density than honeycombs, which is paid by higher pressure drops, fragility under operating conditions and difficulty in the deposition of the active phase layer.

As shown in Table 1 the cell density of foams (3–10 cells/mm^2) is one order of magnitude higher than honeycombs (0.3–1.9 cells/mm^2), due to the smaller attainable diameter of the pores. The void fraction (ε) exhibits a weak dependence on pore diameter (d_p), and is always around 85%, with the exception of 200 and 400 cpsi honeycombs, where it is lower (54 and 74%, respectively) due to the larger wall thickness (Table 1). The specific geometrical surface (S_v) depends on the inverse of d_p. For foams S_v can be calculated according to the cubic cell model (Eq. (1), [10]), and depends linearly on the square root of the solid fraction. For honeycomb monoliths S_v is calculated according to the hollow cylinders model (Eq. (2)), and depends linearly on ε. The highest values of S_v are attained in foams (between 6.2 and 12.4 mm^{-1}), while in honeycomb monoliths it ranges between 1.6 and 5 mm^{-1} (Table 1).

$$S_v = \frac{2[3\pi(1-\varepsilon)]^{1/2}}{d_p} \quad (1)$$

$$S_v = \frac{4\varepsilon}{d_p} \quad (2)$$

Tortuosity and randomness of the foam structure determine not only different geometrical properties with respect to honeycomb monoliths, but also critical differences in the fluid flow in the reactor.

Table 1 reports the values of the effective Reynolds number (Re), the axial Peclet number (Pe_{ax}) defined as the ratio of the characteristic time of axial dispersion and of axial convection and the radial Peclet number (Pe_{rad}) defined as the ratio of the characteristic time of radial dispersion and of axial convection, calculated under the conditions of the experimental runs (with the linear velocity in the empty tube of 6 cm/s at standard conditions).

Re is always below 20 and it is higher for honeycomb monoliths, due to the higher d_p. The straight parallel channels of honeycomb monoliths favor the rapid establishment of a fully developed laminar flow, while the tortuous and random pathways in foams prevent the attainment of a developed flow, notwithstanding the low Re.

Axial and radial dispersion coefficients are calculated according to the correlations reported in Ref. [11]: for honeycombs the dispersion coincides with the molecular diffusivity; for foams (assimilated to packed beds of high porosity) it is enhanced both in axial and radial direction.

Remarkably, in the axial direction, the characteristic convection time is always sufficiently smaller than the dispersion time ($Pe_{ax} > 50$), with the consequence that back-diffusion is always negligible also in foams, despite their higher axial dispersion.

Pe_{rad} gives an evaluation of the radial gradients. In foams, transverse dispersion is favored both by the random and tortuous structure and by the small dimensions of pores, leading to Pe_{rad} from 5 to 20 times smaller than unity. The honeycomb structure and the larger dimension of the cells instead reduce the extent of radial dispersion, with Pe_{rad} around unity for 200 and 400 cpsi, and slightly smaller for the other cell densities (Table 1). These results suggest that significant radial gradients should be expected especially for honeycomb monoliths.

The values of the hydrodynamic entry length (L_{hy}) for the development of a parabolic profile, evaluated according to

Table 1
Geometric and fluid dynamic characteristics of the monolithic supports tested

Morphology	Cell density (cells/mm^2)	d_p (mm)	S_v (mm^{-1})	ε (%)	Re	Pe_{ax}	Pe_{rad}	L_{hy} (mm)	hS_v (J/(s mm^3 K))
Foam (ppi)									
45	3.14	0.42	6.2	84	4	74.1	0.18	0.30	3.9
60	5.58	0.31	8.2	83	3	98.1	0.095	0.20	6.8
80	9.92	0.21	12.4	83	2	122.3	0.048	0.13	15.0
Honeycomb (cpsi)									
200	0.31	1.31	1.6	54	17	53.4	1.63	1.74	0.3
400	0.62	1.09	2.7	74	10	58.2	0.90	1.07	0.6
600	0.93	0.96	3.6	86	8	49.3	0.53	0.87	0.9
900	1.40	0.78	4.4	86	6	51.8	0.35	0.66	1.4
1200	1.86	0.67	5.0	83	6	54.3	0.26	0.55	1.8

d_p, mean pore diameter; S_v, specific geometrical surface; ε, open void fraction; h, heat transfer coefficient; L_{hy} = hydrodynamic entry length.
$Pe_{ax} = \frac{\tau_{disp,ax}}{\tau_{conv}} = \left(\frac{L^2}{D_{ax}}\right)\left(\frac{L}{u}\right)^{-1} = \frac{uL}{D_{ax}}$;
$Pe_{rad} = \frac{\tau_{disp,rad}}{\tau_{conv}} = \left(\frac{d_p^2}{D_{rad}}\right)\left(\frac{L}{u}\right)^{-1} = \frac{ud_p^2}{D_{rad}L}$;
where L is the monolith length, u the surface velocity, D_{ax} and D_{rad} are the axial and radial dispersion coefficients.

Eq. (3) [12], are also reported in Table 1.

$$\frac{L_{hy}}{d_p} = \frac{0.60}{0.035Re + 1} + 0.056Re \quad (3)$$

For low Re values, the order of magnitude of L_{hy} is 1 diameter from the inlet in any case. For honeycomb monoliths it means that the entrance effects extend to roughly one-tenth of the total length. For foam monoliths, it can be expected that the entrance effects are renewed at any interconnection between spherical-like cells, whose characteristic dimension (d_p) is roughly the same of L_{hy}. Here the continuous detachment and formation of the momentum, heat and mass boundary layers determine an increase of the interphase heat and mass transfer efficiency. Table 1 reports hS_v, where h is the average heat transfer coefficient calculated from the Hawthorn's correlation [13], which has a limited validity when a surface reaction takes place at the walls [14], but is a reasonable approximation for a rough evaluation of transfer efficiency. The characteristic length in Hawthorn's correlation is the actual monolith length for honeycombs and the pore diameter for foams. Resulting hS_v values are roughly one order of magnitude higher in reticulated rather than in parallel channel structures.

3. Results

3.1. Experimental tests

The experimental results obtained in this work are presented in Fig. 1, where each catalyst performance is expressed in terms of ethane conversion, ethylene selectivity and yield as a function of the feed ratio C_2H_6/O_2, and in Fig. 2, in the form of conversion versus selectivity plot.

In general, at varying the type of active site and support morphology, ethane conversion maintains the same qualitative trend, progressively decreasing with the increase of the C_2H_6/O_2 ratio. In fact, on increasing the oxygen content in the feed, the autothermal catalytic reactor attains progressively higher operating temperatures (not shown), which in turn boosts both heterogeneous and homogeneous reactions consuming ethane.

On $LaMnO_3$-based monoliths very high ethane conversions can be attained, close to 100%, while on Pt the highest conversion is always lower than 90%. In addition, also ethylene selectivity exhibits the same qualitative trend for the different morphologies on both catalysts (Fig. 1). For all the systems tested selectivity to C_2H_4 progressively increases with increasing the feed ratio up to $C_2H_6/O_2 = 2.25$, slightly above the stoichiometric value for ODH, and then tends to level off or to eventually decrease.

The highest ethylene selectivities are around 74% for $LaMnO_3$ and 67% for Pt, and are always attained at intermediate ethane conversion (around 60–70%), as shown in Fig. 2. From mechanistic considerations, large ethane conversion is attained with oxygen contents larger than stoichiometric for oxidative dehydrogenation ($C_2H_6/O_2 = 2$), which depress ethylene selectivity, instead favoring CO_x formation. Moreover, the higher temperatures reached at low C_2H_6/O_2 ratios also lead to the degradation of ethylene formed towards more stable products, such as CH_4 and C_2H_2. This is clearly shown in Figs. 3 and 4, where the main by-products are reported as a function of ethane conversion respectively on Pt- and $LaMnO_3$-based catalysts. CO, C_2H_2 and CH_4 selectivities all increase with ethane conversion, while only CO_2 selectivity decreases, because its formation is favored at low temperature and hence at lower oxygen content [7]. On the other hand, at exceedingly low oxygen content the exothermicity of the mixture is unable to sustain the high temperatures required for ethylene formation, again determining a decrease of ethylene

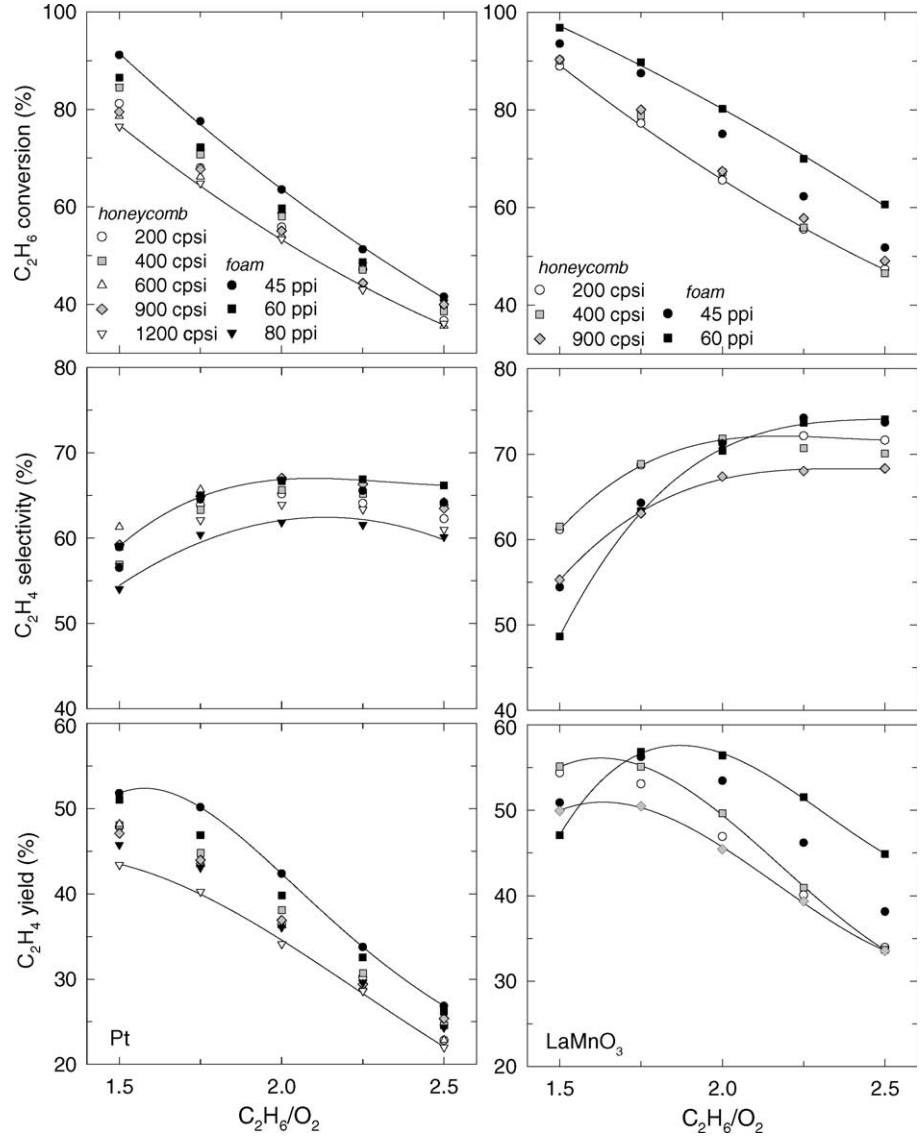

Fig. 1. C_2H_6 conversion, C_2H_4 selectivity and yield as a function of C_2H_6/O_2 feed ratio on Pt and $LaMnO_3$-based monoliths for different morphologies and cell densities (Table 1).

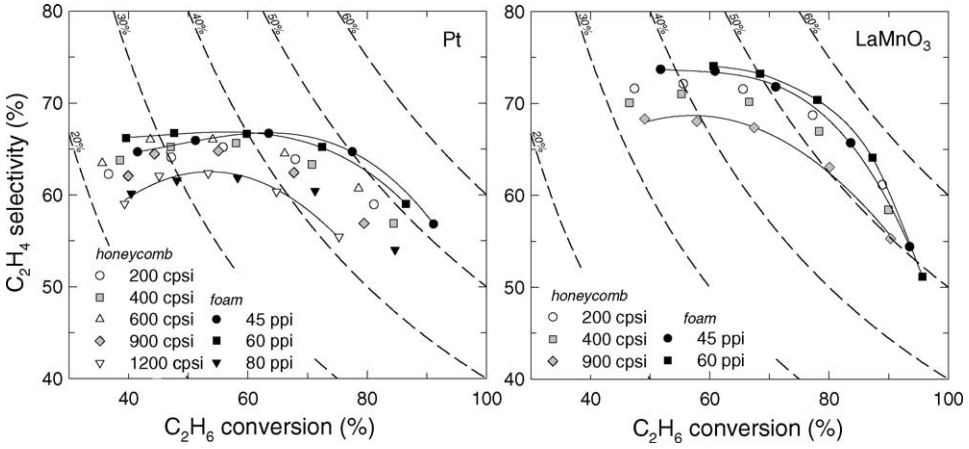

Fig. 2. C_2H_4 selectivity as a function of C_2H_6 conversion on Pt and $LaMnO_3$-based monoliths for different morphologies and cell densities (Table 1).

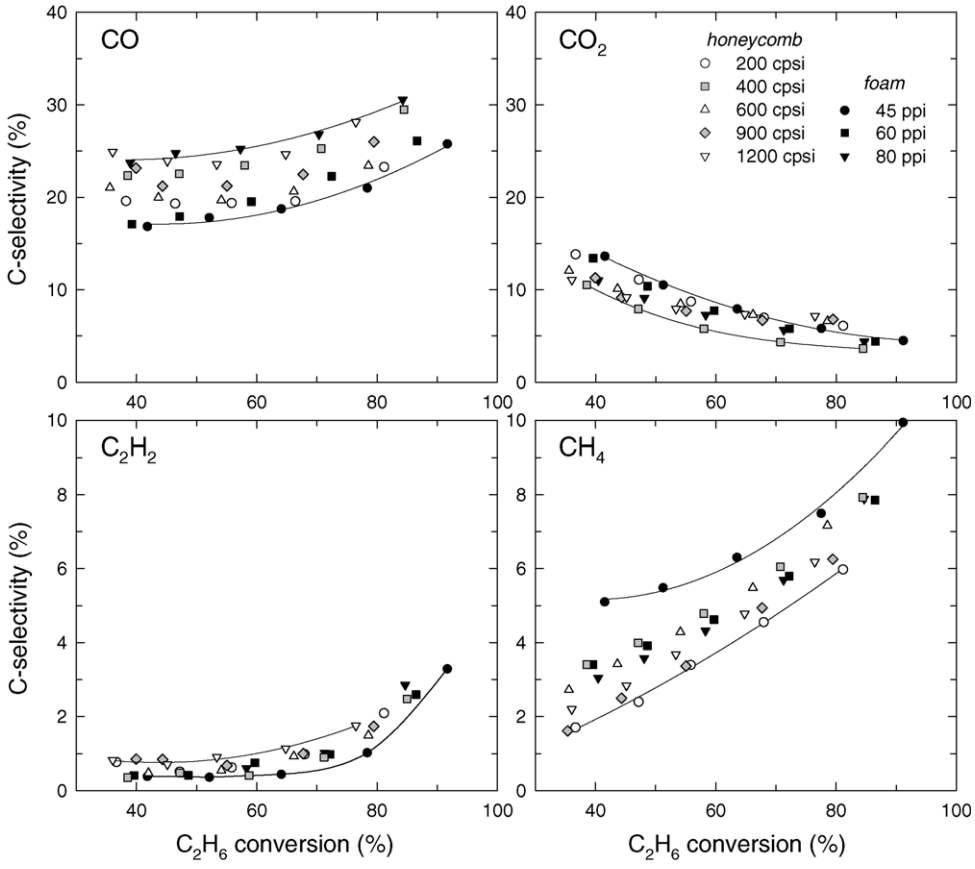

Fig. 3. Carbon atom selectivity of the main by-products as a function of C_2H_6 conversion on Pt-based catalysts for different morphologies and cell densities (Table 1).

selectivity. The sum of these causes determines a maximum of C_2H_4 yield clearly observed on both catalysts for C_2H_6 conversions between 80 and 90% (Fig. 2).

By comparing products distribution on Pt and $LaMnO_3$ catalysts (Figs. 3 and 4), it emerges that much more CO is produced on Pt (8–15 points% of selectivity) than on perovskite, which in turn gives more CO_2 (5–7 points%) and slightly more CH_4 (1–2 points%). Therefore, the superiority of $LaMnO_3$ consists in reducing the amount of sacrificial ethane that has to be oxidized in order to self-sustain the reactor temperature and drive the endothermic ethylene formation, by maximising ethane oxidation to CO_2. Indeed, as shown in Fig. 1, the highest C_2H_4 yield is attained in correspondence of the lowest values of the feed ratio on Pt systems, whereas on $LaMnO_3$ catalysts for C_2H_6/O_2 between 1.75 and 2. Such circumstance bears important process implications, since less oxygen is needed in the feed to obtain an higher yield, thus reducing costs and enhancing productivity.

Coming to the effect of support morphology, the gap between the best and the worst performance for both catalyst compositions is always comprised within 5–10 points% of ethylene selectivity at any ethane conversion (Fig. 2), which is larger than the experimental error. Interestingly, ethylene selectivity on $LaMnO_3$ is always around 10 points% higher than on Pt at parity of support, and the lowest ethylene selectivity curve for $LaMnO_3$ (honeycomb, 200 cpsi) is anyway higher than the best curve for Pt (foam, 45 ppi).

In general, it appears that on foam structures higher ethane conversions can be attained than on honeycombs at any fixed feed ratio, whereas the pore diameter seems to play a minor but contrasting role. In addition, the ethylene selectivity curves in Fig. 2 are roughly ordered in the same way moving from one support to the other for any ethane conversion.

The overall performance of each catalyst in the range of experimental conditions investigated can be assessed in terms of maximum attained ethylene yield for any morphologies and characteristic dimension of the pores of the monolith substrate (Fig. 5). Remarkably, both on foams and honeycombs, the maximum C_2H_4 yield exhibits a maximum at intermediate values of d_p in their respective ranges.

On Pt catalysts, foam supports with 45 and 60 ppi cell density give the best results, with a yield as high as 50% in correspondence to a selectivity of 65%. With the same supports a similar yield is also attained at higher conversion, but selectivity drops to 58%.

Also on $LaMnO_3$ the best performance is reached for foam monoliths (45 and 60 ppi), with 56% ethylene yield and 70% selectivity. A yield larger than 50% is attained on

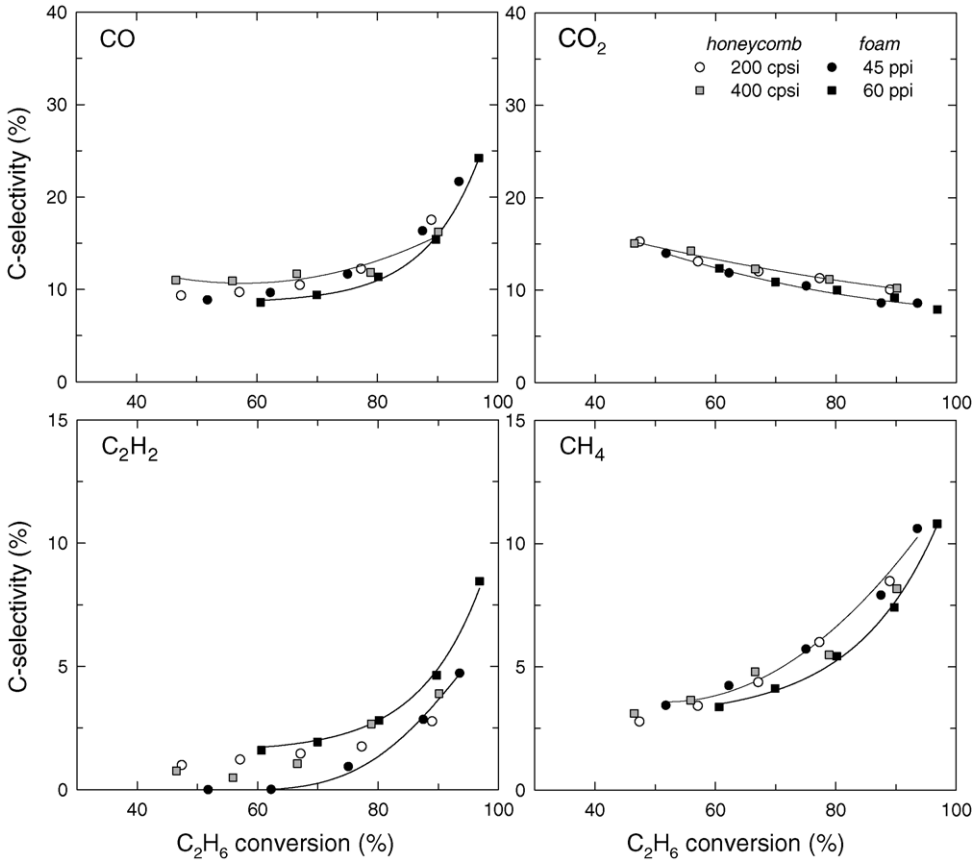

Fig. 4. Carbon atom selectivity of the main by-products as a function of C_2H_6 conversion on $LaMnO_3$-based catalysts for different morphologies and cell densities (Table 1).

any support tested for an ethane conversion comprised between 70 and 90%.

For Pt the following order can be established:

45 ppi, 60 ppi > 600 cpsi, 400 cpsi, 200 cpsi > 900 cpsi, 80 ppi > 1200 cpsi.

For $LaMnO_3$, the same ordering applies limited to the supports tested in the present work.

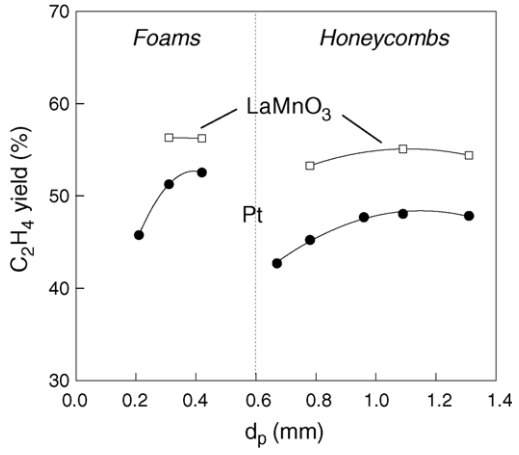

Fig. 5. Maximum C_2H_4 yields obtained on Pt and $LaMnO_3$-based catalysts as a function of pore diameter for foam and honeycomb supports (Table 1).

The strong dependence on active phase and on catalyst support, highlighted in Fig. 2, should be explained in terms of the nature of the mechanism, with the strict coupling between the homogeneous and heterogeneous chemistry by means of interphase heat and mass transfer. The higher performance of foams may be justified in terms of higher mass and heat transfer rate (Table 1). On the other hand Fig. 3 suggests that the degradation of performance observed for 1200 cpsi and 80 ppi is caused by the predominance of the heterogeneous chemistry, with the formation of 10 points% more CO than over the best supports. Such effect is less pronounced on $LaMnO_3$, which is a better deep oxidation catalyst than Pt, with a lower tendency to form syngas even at very high values of S_v (Fig. 2).

The reason for the attainment of the highest performance at an intermediate pore dimension (45–60 ppi for foams, 400–600 cpsi for honeycombs), with relevant reduction of ethylene selectivity at higher cell density (especially at 80 ppi and 1200 cpsi) deserves further understanding.

3.2. Numerical model

A mathematical model, previously adopted in the investigation of the hetero-homogeneous ethane ODH reaction [15], is herein used to study the effect of the channel diameter and to get insights on the causes of the

experimental finding of an optimum at intermediate pore dimensions.

A honeycomb monolith is modeled as a straight axi-symmetric cylindrical channel with adiabatic zero-conductivity walls and adopting the boundary layer approximation ($Pe_{ax} \gg 1$). The surface kinetics is lumped in a single step reaction rate of consumption of C_2H_6 to CO_2 and H_2O. This implies that the catalytic reaction of species such as C_2H_4, C_2H_2, CH_4, CO and H_2, which may be present in significant fractions in the bulk phase, and the formation and destruction of radicals on the walls are neglected. Catalyst contribution is undoubtedly oversimplified in the case of Pt, where the surface formation of products of partial oxidation of ethane, such as CO and H_2, is favored with respect to the formation of CO_2 and H_2O, but it is a reasonable approximation in the case of $LaMnO_3$ catalyst, where ethane oxidation always occurs with higher CO_2 selectivity (this work, [5]).

The channel diameter d_p is varied between 0.1 and 1.0 mm, maintaining constant the inlet superficial velocity (u_{in} = 30 cm/s at standard conditions), hence assuming a constant void fraction at varying d_p, and constant inlet fuel to oxygen ratio ($C_2H_6/O_2 = 2$), N_2 dilution (30 vol.%) and temperature (500 °C). Fig. 6 reports the computed axial profiles of wall and bulk gas temperature, bulk O_2 and C_2H_6 conversions and CO_2 and CO carbon atom yields, at varying d_p. The bulk variables (φ_b) are calculated as average along the radius: $\varphi_b = \int_0^R \rho v_z \varphi r \, dr / \int_0^R \rho v_z r \, dr$.

The reduction of d_p leads to the increase of the specific geometrical surface (S_v) and to the increase of the mass and heat transfer rate (Table 1), with the consequence that the surface reaction (largely under external diffusion regime) becomes dominant with respect to the homogeneous path until the oxidant is fully consumed.

The wall temperature (T_{wall}) rises more rapidly for larger d_p, due to the lower heat transfer efficiency between the surface and the bulk gas phase. Hence, the light-off point of heterogeneous reactions occurs closer to the entrance of the catalytic monolith.

Also the onset of gas phase reactions occurs closer to channel inlet section for larger d_p. This is clearly shown in Fig. 6 by a change in slope of the axial profiles of T_{bulk}, O_2 and C_2H_6 conversions and by the formation of CO. Indeed, according to the model CO is produced exclusively in the gas phase, in contrast to CO_2, which is formed mainly through the surface reaction. The reaction mechanism switches from purely heterogeneous to hetero-homogeneous at relatively low oxygen conversions (below 30%), determining high CO yields, which in turn limit C_2H_4 formation.

Conversely, at lower values of d_p, the onset of the gas phase reactions occurs at almost complete O_2 conversion (95%): for this reason a lower selectivity to CO is found at the exit of the reactor.

At higher d_p, the simultaneous occurrence of the heterogeneous (exothermic) and the homogeneous (mainly endothermic) reactions in conjunction with the lower heat transfer efficiency from the surface, determines a smooth increase of T_{bulk} to a peak below 1100 °C. Instead, for d_p = 0.1 and 0.2 mm, the bulk gas temperature rise is steeper, since the heat produced by the surface reaction is more efficiently transferred to the gas before the onset of the homogeneous reactions, and the maximum T_{bulk} ranges between 1170 and 1250 °C.

The different profiles of temperature and O_2 concentration are reflected on product distribution, which is shown in Fig. 7 versus the reaction coordinate (ethane conversion), in terms of carbon atom selectivity of the main products,

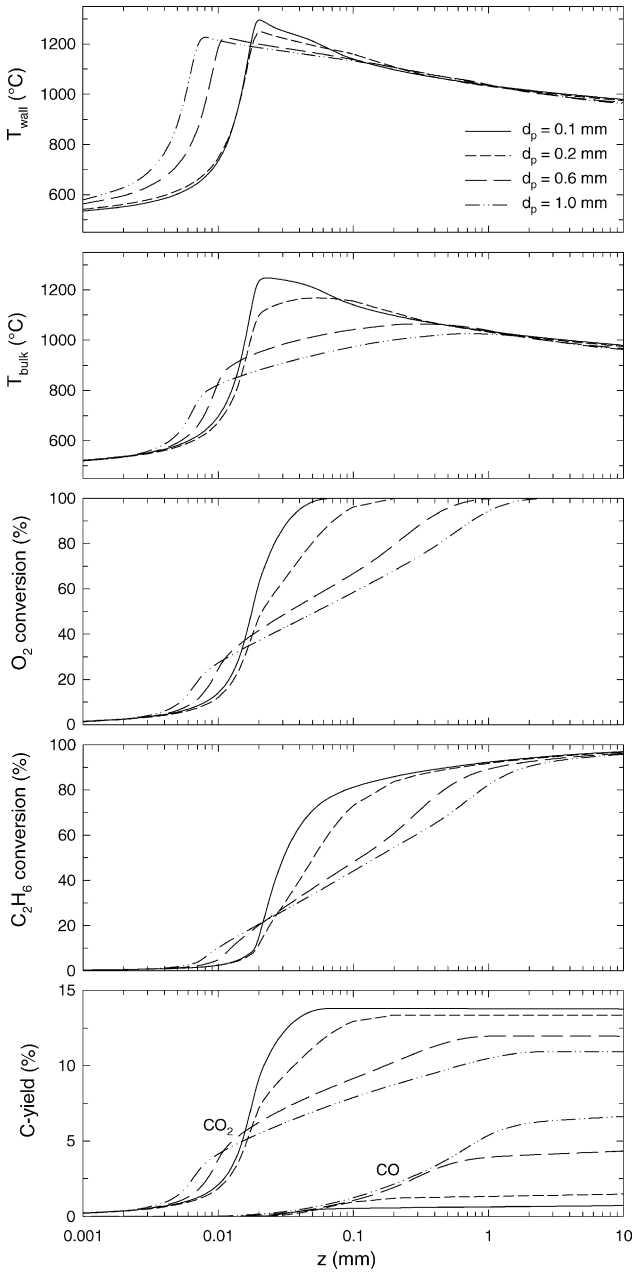

Fig. 6. Computed values of wall temperature (T_{wall}), bulk gas temperature (T_{bulk}), O_2 and C_2H_6 conversions and CO_2 and CO carbon-yields along the axial coordinate z at varying d_p.

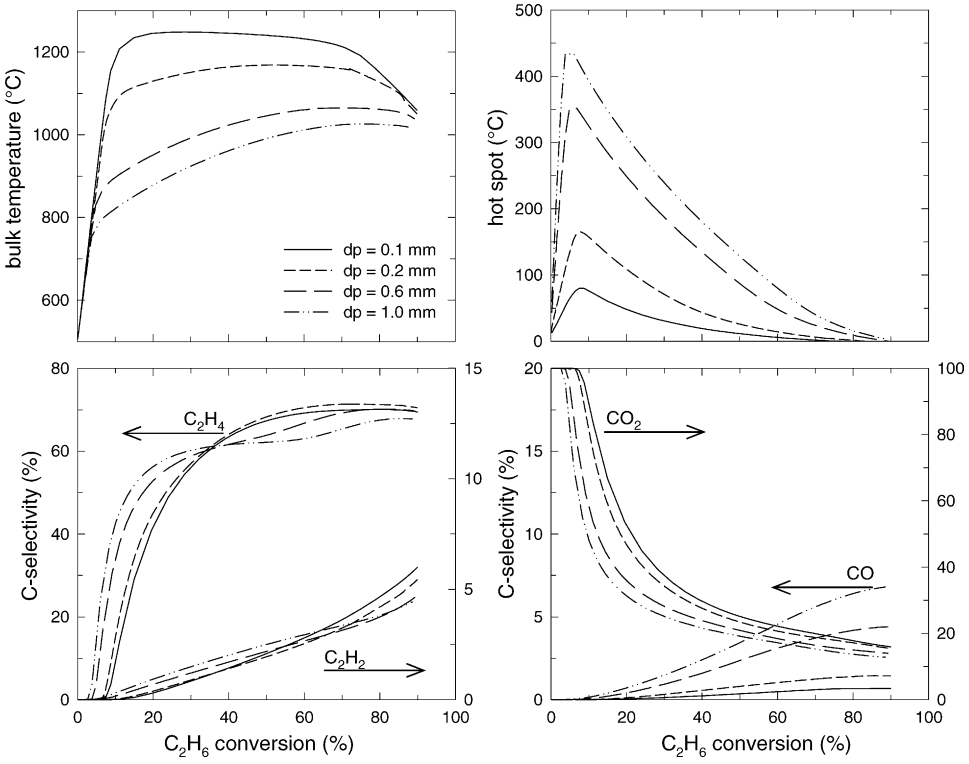

Fig. 7. Computed values of bulk temperature, hot spot ($T_{wall} - T_{bulk}$), and radial averaged carbon atom selectivity of the main products as a function of C_2H_6 conversion at varying d_p.

together with the bulk temperature and the hot spot. Ethane conversion along the channel is chosen as abscissa in all plots of Fig. 7 in order to better visualize the trends and to assist in the comparison at varying d_p.

At high values of d_p the slower heat transfer rate determines steep radial temperature gradients and local over-heating, as confirmed by the formation of higher hot spot ($T_{wall} - T_{bulk}$) at the wall and lower bulk gas temperature (Fig. 7). The hot spot is always positioned at the ignition of gas phase reactions but its value is roughly 450 °C for $d_p = 1$ mm, while it is reduced to 50 °C for $d_p = 0.1$ mm, even though the wall catalyst temperature does not differ for more than 100 °C.

Furthermore, since for larger d_p the homogeneous reactions proceed in concurrence to the heterogeneous reactions, the formation not only of C_2H_4, but also of C_2H_2 (Fig. 7), CH_4, C_3 and C_4 hydrocarbons via endothermic reaction paths of dehydrogenation, cracking and reformation occurs. In this case, since O_2 conversion is low at the ignition of gas phase reactions (Fig. 6), a significant fraction of ethane is oxidized also in the gas phase, leading to the observed higher CO selectivity for larger d_p (Fig. 7).

At low d_p (0.2 and 0.1 mm) the surface reaction and the interphase mass and heat transfer rates are faster, with the consequence that the homogeneous reactions are ignited at higher ethane conversion and the hot spots are reduced. Most of the oxygen is hence consumed via the heterogeneous reaction (Fig. 6), leading to a higher CO_2 selectivity, with the minimization of the fraction of ethane sacrificed in oxidation reactions. On the other hand, a higher T_{bulk} is attained, with the consequence that the formation of C_2H_2, CH_4 and higher hydrocarbons (C_3–C_4) takes place at higher ethane conversion, but with higher selectivity. Acetylene selectivity, illustratively reported in Fig. 7, exhibits an increasing trend at high ethane conversion when reducing d_p.

It can be concluded that at low d_p ethylene is formed under more favorable conditions (higher bulk temperature and lower oxygen content) with higher selectivity (above 70%) already from 35% ethane conversion. However, the exceedingly high value of the gas temperature leads to side reactions, which in turns reduce the ethylene selectivity. The two effects counterbalance, determining the attainment of same values of C_2H_4 selectivity at $d_p = 0.1$ and 0.6 mm, while the best performance is reached at an intermediate value of d_p (0.2 mm).

Hence the key parameters in determining ethylene selectivity and yield are represented by the gas temperature and by the activation of the homogeneous reaction, which can be controlled by regulating the heat transfer efficiency and the homogeneous–heterogeneous ratio. These conclusions are herein specifically obtained for honeycomb monoliths, but are also qualitatively pertinent to foams.

4. Conclusion

The oxidative dehydrogenation of ethane to ethylene occurs in short contact time reactors via complex coupling between heterogeneous and homogeneous reactions and

interphase heat and mass transfer. Hence in the optimization of the process, not only catalyst composition issues must be taken into account, but also the reactor morphology, which regulates the contact surface between gas and catalyst, the fluid dynamics and the void fraction where homogeneous reactions occur.

Experimental results showed that, even though ethylene formation occurs in the gas phase, the catalyst composition outscores any morphological consideration. $LaMnO_3$-based catalysts always give higher performance than Pt-based ones independently on the support.

Nevertheless, support morphology and cell density may affect ethylene selectivity for more than 10 points%. It can be generally stated that foams perform better than honeycombs thanks to the higher geometrical surface and to the high degree of tortuosity and randomness of the pores, which drastically increase the heat and mass transfer rate.

In contrast with the results reported by Bodke et al. [2], the best performance is not attained for the highest values of S_v. The 45 and 60 ppi foams gave the highest ethylene selectivity and yield, even though the performance of 400 and 600 cpsi honeycomb monoliths is only slightly lower. Hence, at increasing cell density above these optimal values both for foams and for honeycombs, the performance decreases.

The mathematical model highlighted that the coupling of heterogeneous and homogeneous reactions is controlled by interphase mass and heat transfer and the optimal conditions for ethylene formation and preservation are attained at an intermediate value of the channel dimension.

Based on the evaluation of the performance, it appears that 45 and 60 ppi foam monoliths are the optimal supports for the ODH reaction. Nevertheless, honeycomb monoliths guarantee significant advantages with respect to foams in terms of pressure drops, structural strength and easier catalyst deposition, resulting only in a minor reduction in performance for 400 and 600 cpsi cell density.

Hence, the choice of the optimal support should be driven by a tradeoff analysis among performance, pressure drops, structural strength and ease of catalyst deposition.

Acknowledgments

The authors wish to thank Vitale Stanzione and Gabriella Callegaro for the experimental campaign.

References

[1] M. Huff, L.D. Schmidt, J. Phys. Chem. 97 (1993) 11815.
[2] A.S. Bodke, S.S. Bharadwaj, L.D. Schmidt, J. Catal. 179 (1998) 138.
[3] V.A. Sadykov, S.N. Pavlova, N.F. Saputina, I.A. Zolotarskii, N.A. Pakhomov, E.M. Moroz, V.A. Kuzmin, A.V. Kalinkin, Catal. Today 61 (2000) 93.
[4] R. Lødeng, O.A. Lindvåg, S. Kvisle, H. Reier-Nielsen, A. Holmen, Appl. Catal. A 187 (1999) 25.
[5] F. Donsì, R. Pirone, G. Russo, J. Catal. 209 (2002) 51.
[6] F. Donsì, R. Pirone, G. Russo, Catal. Today 91–62 (2004) 285.
[7] F. Donsì, S. Cimino, R. Pirone, G. Russo, Ind. Eng. Chem. Res. 44 (2005) 285.
[8] J.T. Richardson, Y. Peng, D. Remue, Appl. Catal. A 204 (2000) 19.
[9] M.V. Twigg, J.T. Richardson, Trans. I Chem. E 80 (2002) 183.
[10] L. Giani, G. Groppi, E. Tronconi, Ind. Eng. Chem. Res. (3 August 2005) in press.
[11] C.Y. Wen, L.T. Fan, Models for Flow Systems and Chemical Reactors, Marcel Dekker Inc., New York, 1975 , p. 113.
[12] R.K. Shah, A.L. London, Laminar Flow Forced Convection in Ducts, Academic Press, New York, 1978 , p. 98.
[13] R.D. Hawthorn, AIChE Symp. Ser. 70 (1974) 428.
[14] A. Di Benedetto, F.S. Marra, G. Russo, Chem. Eng. Sci. 58 (2003) 1079.
[15] F. Donsì, T. Caputo, A. Di Benedetto, R. Pirone, G. Russo, AIChE J. 50 (2004) 2233.